# ChemComm

## Accepted Manuscript

This article can be cited before page numbers have been issued, to do this please use: Z. Yang, H. Lin, J. Huang, A. Li, C. Sun, J. Richmond and J. Gao, *Chem. Commun.*, 2019, DOI: 10.1039/C9CC01816F.




ROYAL SOCIETY OF CHEMISTRY

rsc.li/chemcomm

View Article Online
DOI: 10.1039/C9CC01816F

Journal Name

COMMUNICATION

# A gadolinium-complex-based theranostic prodrug for *in vivo* tumour-targeted magnetic resonance imaging and therapy

Zhaoxuan Yang,[a‡] Hongyu Lin,[a‡] Jiaqi Huang,[a‡] Ao Li,[a] Chengjie Sun,[a] Jonathan Richmond,[b] and Jinhao Gao[a]*

Received 00th January 20xx,
Accepted 00th January 20xx

DOI: 10.1039/x0xx00000x

www.rsc.org/



**Here we report a target-specific theranostic prodrug (1a) containing Gd-DOTA, biotin, and camptothecin (CPT) along with a disulfide self-immolative linker. This prodrug features selective targeting towards tumour cells and tissues, stimuli-responsive controlled release, enhanced anticancer efficacy, and accurate diagnosis and real-time monitoring *via* contrast-enhanced magnetic resonance imaging (MRI).**

Many types of treatment have been developed for various cancer, such as surgery, immunotherapy,[1] targeted radiation,[2, 3] and gene therapies.[4] In spite of 100-year medical advancement since its discovery, chemotherapy remains the frontline therapy for many types of cancer, used in conjunction with surgical treatment. However, the main challenge of chemotherapy is its inability to selectively eliminate tumour cells and leave healthy cells undamaged. Ideally, we would be able to administer a drug *in vivo* at the perfect dose, resulting in selective damage to tumour cells only. In attempt to achieve this, small conjugate-based theranostic agents have been developed.[5] These agents could selectively release chemotherapeutic agents at tumour sites and achieve both diagnosis and therapy, which meet the needs of personalized and precise medicine.[6, 7] Among these agents, theranostic prodrugs based on fluorescence imaging have been extensively studied.[8-15] Fluorescence imaging can accomplish high sensitivity at cellular level. However, due to its limited penetration and poor ability to provide anatomy details, it has difficulties in accurate tumour diagnosis and detailed treatment monitoring.[16] This severely restricts its application *in vivo*. Moreover, many commonly used organic fluorophores, such as coumarin, BODIPY, Rhodamine, and cyanine, suffer from poor water solubility, which is often a challenging issue to address during the development of theranostic prodrugs by integrating fluorescent dyes and chemotherapeutic drugs.

Magnetic resonance imaging (MRI) is a non-invasive imaging technique widely used in clinical practice. MRI is able to offer high-definition images of an entire organism with deep penetration and detailed anatomical information.[16, 17] Therefore, theranostic agents based on MRI could achieve not only sensitive and accurate diagnosis, but also accomplish *in vivo* real-time monitoring, which provides invaluable information for precise assessment of the therapeutic outcomes and better understanding of the biodistribution and pharmacokinetics of drugs.[18, 19] Various MRI-based nanoparticulate theranostic systems have been developed.[17, 20, 21] However, several barriers including homogeneity, reproducibility, and pharmacokinetics need to be overcome during the translation of these systems from bench to bedside. In contrast, molecular theranostic conjugates with a precise structure, repeatable synthesis, and ease of adaptation, offer a more promising prospect in both preclinical and clinical contexts.

Herein, we designed a molecular theranostic prodrug **1a** (Figure 1a), which contains a targeting agent biotin, a modified gadolinium (III)-1,4,7,10-tetraazacyclododecane-1,4,7,10-tetraacetate (Gd-DOTA) complex, and an anticancer drug camptothecin (CPT). Biotin receptors (sodium-dependent multivitamin transporter, SMVT) are overexpressed on the cell surface of many cancer cells, including HeLa and A549, which renders biotin appealing as a targeting unit to boost the drug efficacy.[22] Gd-DOTA is a commonly used contrast agent for clinical MRI, offering considerable contrast enhancement which significantly increases both the sensitivity and accuracy of MRI.[23, 24] Camptothecin (CPT), a potent topoisomerase I inhibitor,[25] is one of the most effective antitumour drugs with promising developmental prospects. However, clinical applications of CPT have been restricted due to its poor water solubility and adverse side effects.[26] The incorporation of highly

[a] *State Key Laboratory of Physical Chemistry of Solid Surfaces, The Key Laboratory for Chemical Biology of Fujian Province and Department of Chemical Biology, College of Chemistry and Chemical Engineering, Xiamen University, Xiamen 361005, China. *E-mail: jhgao@xmu.edu.cn*
[b] *Chemical Nanoscience Laboratory, School of Natural and Environmental Sciences, Newcastle University, Newcastle-Upon-Tyne, NE1 7RU, United Kingdom.*
‡ These authors contributed equally to this work.
† Electronic Supplementary Information (ESI) available: The experimental details and Figures S1-S3 See DOI: 10.1039/x0xx00000x

hydrophilic Gd-DOTA would greatly improve the water solubility of **1a** and hence reduce the uptake *via* passive diffusion in normal cells.[27] At the same time, the increase in hydrophilicity would also enhance biotin receptor-mediated endocytosis.[28] The use of a disulfide self-immolative linker would further increase the selectivity as the reductive environment inside tumour cells would facilitate the release of CPT. Last but not the least, the fluorescence of CPT would be quenched due to the presence of paramagnetic Gd-DOTA,[17] which offers a complementary approach to monitor drug release with a "turn-on" fluorescence signal (Figure 1a) apart from the major means of diagnosis and monitoring *via* MRI.

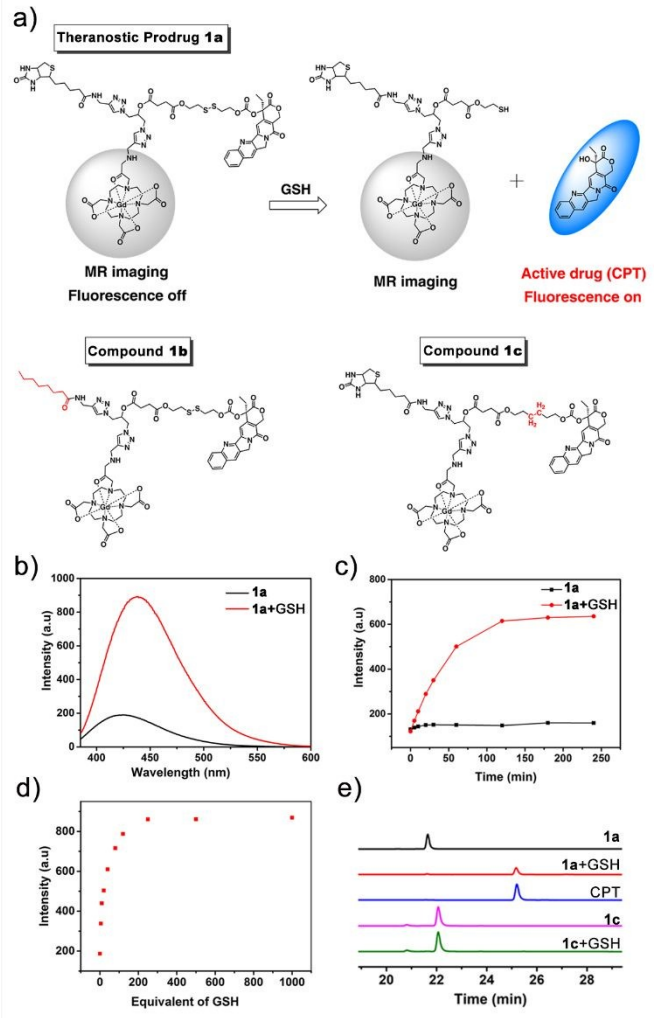


**Figure 1.** (a) The mechanism for the releasing of CPT from **1a** and the structures of control molecules **1b** and **1c**. (b) Fluorescence spectra of **1a** (5 μM) incubated with or without GSH (5 mM) in PBS (pH 7.4) for 3h. (c) Fluorescence spectra of **1a** (5 μM) incubated with GSH (5 mM) in PBS over time. (d) Fluorescence intensities of **1a** (5 μM) incubated with different concentrations of GSH in PBS. (e) HPLC chromatograms of CPT, **1a** (10 μM) and **1c** (10 μM) incubated with or without GSH (1 mM) in PBS for 3 h.

## RESULTS AND DISCUSSION

We constructed **1a** with a modular strategy using epichlorohydrin as the central piece (Scheme S1), which facilitates preparation of the controls, **1b** and **1c** (Figure 1a). The targeting component biotin is absent in **1b**, while **1c** lacks the disulfide bond, preventing the release of CPT in reducing environments. Detailed synthesis and characterization of **1a**, **1b,** **1c** and the intermediates are shown in the Electronic Supporting Information (Figure S1).

The fluorescence of CPT was significantly quenched in the prodrug **1a** (Figure 1b), most likely due to the presence of paramagnetic Gd-DOTA. Upon treatment with GSH, which cleaves the disulfide bond and discharges CPT, the fluorescence was recovered (Figure 1b). This was exploited to monitor the release of CPT. As shown in Figure 1c and 1d, the fluorescence intensity increased by six fold over a period of 4 h after **1a** was treated with excess GSH, clearly demonstrating the GSH-mediated release process of CPT. In contrast, no appreciable change in fluorescence for **1c**, which lacks the cleavable disulfide bond, was observed under the same conditions (Figure S2). To further validate the disulfide cleavage, we performed high performance liquid chromatography (HPLC) to trace the products. Upon incubation with GSH, the original peak for **1a** at 22 min disappeared and a new peak at 25 min appeared, which was confirmed to be free CPT (Figure 1e). On the contrary, treatment of **1c** with GSH showed no apparent change. These results reveal that the disulfide bond in **1a** could be effectively cleaved in reductive environments, which triggers a self-immolative process and releases CPT.

To investigate the targeting ability of the prodrug **1a**, we took the advantage of the "turn-on" fluorescence of released CPT. Fluorescence microscopy showed that the fluorescence intensity of biotin receptor (BR) overexpressed cancer cells (HeLa and A549) was much higher than that of normal cells (MRC-5 and HL7702) after treatment with **1a** for 15 min (Figure 2a), indicating the higher uptake of **1a** for BR overexpressed cancer cells (Figure S3). When HeLa and A549 cells were incubated with biotin before treatment with **1a**, the fluorescence intensity was significantly attenuated (Figure 2b), suggesting that biotin could block the uptake of **1a** and the uptake of **1a** is *via* BR-mediated endocytosis. Moreover, A549 cells treated with **1a** showed significantly higher fluorescence intensity than the cells treated with **1b** or free CPT (Figure 2c, d), validating the excellent targeting ability of the prodrug **1a**.

We also evaluated the contrast-enhanced performance of **1a** for MRI. The longitudinal relaxivity ($r_1$) of **1a** in PBS was calculated to be 8.2 $mM^{-1}s^{-1}$, which is significantly higher than that of Gd-DOTA, a typical clinical CA with $r_1$ of 4.9 $mM^{-1}s^{-1}$ (Figure S4).[29] The excellent $T_1$ relaxivity of **1a** could increase the sensitivity of contrast-enhanced MRI, which provides a better performance for drug monitoring. The *in vitro* cellular uptake of **1a** was visualized by the use of an MRI scanner. We incubated A549 cells with **1a** over a period of 12 h and found that the MR signal gradually intensified as the incubation time increased and reached a maximum at 3 h (Figure 2e), strongly indicating that the time dependent uptake of **1a** may saturate at 3 h.

The cytotoxicities of **1a** against both cancer cells and normal cells were assessed *via* MTT assays. As shown in Table 1, the $IC_{50}$ of **1a** against BR overexpressed cancer cells, A549 and HeLa, was lower than those of free CPT and **1b**, indicating the enhanced cytotoxicity of **1a** (Figure S5). Notably, the $IC_{50}$ of **1a** against

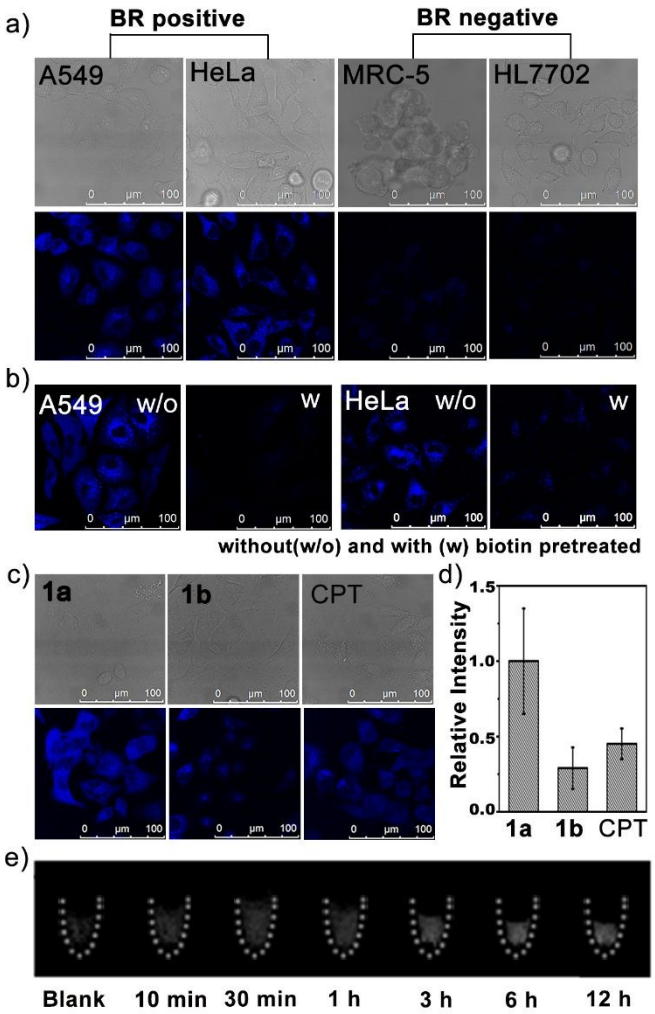


**Figure 2.** (a) Bright-field and fluorescent images of biotin-receptor overexpressed cancer cells (HeLa and A549, BR positive) and normal cells (MRC-5 and HL7702, BR negative). Cells were incubated with **1a** (10 μM) in PBS for 15 min. (b) Fluorescent images of biotin-receptor overexpressed A549 and HeLa cells incubated with **1a** (10 μM) in PBS without or with pre-incubation of biotin (1.5 mM in DMEM with 10% FBS) for 3 h. (c) Bright-field and fluorescent images of A549 cells incubated with **1a**, **1b**, or CPT in PBS for 3 h. (d) Quantitative analysis on the fluorescence intensities of (c). The data were presented as mean ± SD ($n$ = 5/group). (e) $T_1$-weighted MR images of A549 cells incubated with **1a** (20 μM in DMEM with 10% FBS) over a period of 12 h.

A549 was 0.41 μM, only one half of that of free CPT. Interestingly, the cytotoxicity of **1a** against normal cell lines was much lower than those of free CPT and **1b**, suggesting superior selectivity of **1a**. The elevated cytotoxicity and selectivity against cancer cells may be attributed to the introduction of the targeting group biotin, which is consistent with the results of cell uptake experiments (Figure 2, Figure S6). Gene expression profiles (RNA-seq, Figure 3) further revealed that **1a** could up-regulate anti-oncogenes and down-regulate proto-oncogenes and non-small cell lung cancer (NSCLC) associated genes, which is similar to free CPT, indicating that the enhanced cytotoxicity and selectivity of **1a** over free CPT mainly arise from the biotin mediated targeting.

**Table 1.** Cytotoxicity evaluation of **1a**, **1b**, **1c**, and CPT against HeLa and A549 cancer cell lines and MRC-5, HL7702, 293T, and WPMY-1 normal cell lines *via* MTT assays.

| Cell lines | $IC_{50}$ values | | | |
|---|---|---|---|---|
| | **1a** | CPT | **1b** | **1c** |
| A549 [a] | 0.41[q] | 0.79[q] | 2.76[q] | >20.00[q] |
| HeLa [a] | 16.81[q] | 19.82[q] | 18.15[q] | >64.00[q] |
| MRC-5 [b] | >8.00[q] | 1.97 [q] | 1.34[q] | >8.00[q] |
| HL7702 [b] | 60.40[f] | 25.51[f] | 19.70[f] | 1188.00[f] |
| 293T [b] | 114.30[f] | 35.80[f] | 31.00[f] | 5220.00[f] |
| WPMY-1 [b] | 119.20[f] | 33.38[f] | 34.60[f] | 3867.00[f] |

[a] Biotin overexpressed cancer cell lines, [b] normal tissue cell lines. [q] concentration unit μM, [f] concentration unit nM.

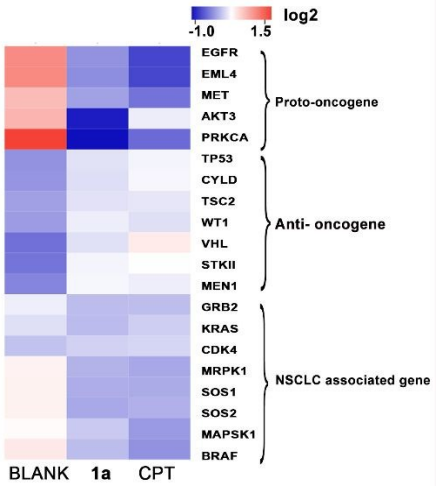


**Figure 3.** The heat map depicting gene expression profiling of A549 cell samples from each group (PBS, **1a**, or CPT treatments). Red and blue colors indicate high and low relative expression levels, respectively.

To evaluate the theranostic function of **1a** *in vivo*, we used nude mice bearing A549 tumours as a model. For imaging performance evaluation, mice were separated into two groups, injected intravenously with **1a** or **1b**, and subjected to $T_1$-weighted MRI. Compared to mice injected with **1b**, mice injected with **1a** showed a much brighter signal in the tumour regions, especially after 1 h post administration (Figure 4a). Quantitative analysis further confirmed that the signal-to-noise ratio (SNR) of the tumour region of mice treated with **1a** was significantly higher than that of mice treated with **1b**, which is highly ascribed to the biotin mediated targeting ability of **1a**. For therapeutic efficacy assessment, mice were separated into three groups and subjected to intravenous injection of PBS, **1a**, or free CPT as indicated (Figure 4c, Figure S7). There was a significant difference in tumour growth between mice treated with **1a** and mice treated with free CPT, indicating the remarkable tumour inhibition ability of **1a** over CPT, which is in agreement with the cell cytotoxicity evaluation. H&E staining showed that the prodrug **1a** had no apparent side effects on normal tissues, but caused necrosis of tumour tissues (Figure S8).

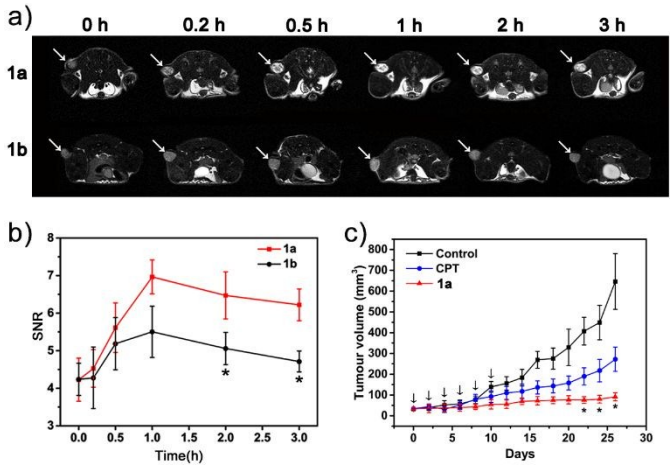


**Figure 4.** (a) $T_1$-weighted MR images of nude mice bearing A549 tumours (indicated by white arrows). **1a** or **1b** (100 μM/Kg body weight, 163 mg/Kg for **1a** and 153 mg/Kg for **1b**) was injected intravenously. Images were acquired on a 7 T MRI scanner. (b) Quantitative analysis on signal-to-noise ratios (SNRs) of tumours (*$p$ < 0.05, $n$ = 4/group). (c) Tumour growth curve of nude mice bearing A549 tumours treated with **1a** (3 mg CPT/kg body weight), CPT (3 mg CPT/kg body weight), or PBS six times for first two weeks (indicated by black arrows). ($n$ = 5 for each group, *$p$ < 0.05 compared to CPT and PBS treatment groups). The tumour size was measured every two days during the treatment period.

In conclusion, we have developed a novel theranostic prodrug **1a** with real-time monitoring *via* MRI, which provides better spatial resolution and soft tissue contrast than the reported theranostic prodrugs relying solely on fluorescence imaging. The prodrug **1a** could selectively target biotin-receptor overexpressed cancer cells with high uptake, effectively release CPT in reducing environments, and kill cancer cells with low $IC_{50}$ values. The excellent $T_1$ contrast-enhanced performance of **1a** enables real-time monitoring of drug uptake in cells and accurate diagnosis of tumour with high sensitivity. Moreover, the prodrug **1a** could achieve a considerable improvement on tumour treatment with higher efficacy and reduced side effects. All these features demonstrate the great potential of **1a** for accurate diagnosis and precise treatment of tumours. This strategy could be easily adapted for other anticancer drugs and would be enlightening for the development of more molecular theranostic agents.

The authors acknowledge the research support from National Natural Science Foundation of China (21771148, 21602186, 21521004, and 81430041), Natural Science Foundation of Fujian Province of China (2018J01011), and Fundamental Research Funds for the Central Universities (20720170020, 20720170088, and 20720180033).

## Conflicts of interest

There are no conflicts of interest.

## Notes and references

1. D. M. Pardoll, *Nat. Rev. Cancer.*, 2012, **12**, 252-264.
2. H. S. Kaplan, *Cancer*, 1977, **39**, 689-693.
3. M. de Jong, W. A. Breeman, D. J. Kwekkeboom, R. Valkema and E. P. Krenning, *Acc. Chem. Res.*, 2009, **42**, 873-880.
4. X. Zhang and W. T. Godbey, *Cancer. Gene. Ther.*, 2011, **18**, 34-41.
5. M. H. Lee, A. Sharma, M. J. Chang, J. Lee, S. Son, J. L. Sessler, C. Kang and J. S. Kim, *Chem. Soc. Rev.*, 2018, **47**, 28-52.
6. S. E. Jackson and J. D. Chester, *Int J Cancer*, 2015, **137**, 262-266.
7. L. J. van't Veer and R. Bernards, *Nature*, 2008, **452**, 564-570.
8. S. Santra, C. Kaittanis, O. J. Santiesteban and J. M. Perez, *J. Am. Chem. Soc.*, 2011, **133**, 16680-16688.
9. S. Maiti, N. Park, J. H. Han, H. M. Jeon, J. H. Lee, S. Bhuniya, C. Kang and J. S. Kim, *J. Am. Chem. Soc.*, 2013, **135**, 4567-4572.
10. Y. Yuan, R. T. Kwok, B. Z. Tang and B. Liu, *J. Am. Chem. Soc.*, 2014, **136**, 2546-2554.
11. M. H. Lee, J. Y. Kim, J. H. Han, S. Bhuniya, J. L. Sessler, C. Kang and J. S. Kim, *J. Am. Chem. Soc.*, 2012, **134**, 12668-12674.
12. R. Kumar, J. Han, H. J. Lim, W. X. Ren, J. Y. Lim, J. H. Kim and J. S. Kim, *J. Am. Chem. Soc.*, 2014, **136**, 17836-17843.
13. R. Weinstain, E. Segal, R. Satchi-Fainaro and D. Shabat, *Chem. Commun.*, 2010, **46**, 553-555.
14. H. Han, W. Teng, T. Chen, J. Zhao, Q. Jin, Z. Qin and J. Ji, *Chem. Commun.*, 2017, **53**, 9214-9217.
15. H. Singh, S. J. Kim, D. H. Kang, H. R. Kim, A. Sharma, W. Y. Kim, C. Kang and J. S. Kim, *Chem. Commun.*, 2018, **54**, 12353-12356.
16. S. Gnaim, A. Scomparin, S. Das, R. Blau, R. Satchi-Fainaro and D. Shabat, *Angew. Chem. Int. Ed.*, 2018, **57**, 9033-9037.
17. M. H. Lee, E. J. Kim, H. Lee, H. M. Kim, M. J. Chang, S. Y. Park, K. S. Hong, J. S. Kim and J. L. Sessler, *J. Am. Chem. Soc.*, 2016, **138**, 16380-16387.
18. T. L. Kalber, N. Kamaly, S. A. Higham, J. A. Pugh, J. Bunch, C. W. McLeod, A. D. Miller and J. D. Bell, *Bioconjug. Chem.*, 2011, **22**, 879-886.
19. Z. Zhu, X. Wang, T. Li, S. Aime, P. J. Sadler and Z. Guo, *Angew. Chem. Int. Ed.*, 2014, **53**, 13225-13228.
20. Z. Zhao, X. Wang, Z. Zhang, H. Zhang, H. Liu, X. Zhu, H. Li, X. Chi, Z. Yin and J. Gao, *ACS Nano*, 2015, **9**, 2749-2759.
21. L. Wang, H. Lin, X. Chi, C. Sun, J. Huang, X. Tang, H. Chen, X. Luo, Z. Yin and J. Gao, *Small*, 2018, **14**, 1801612.
22. S. Chen, X. Zhao, J. Chen, J. Chen, L. Kuznetsova, S. S. Wong and I. Ojima, *Bioconjug. Chem.*, 2010, **21**, 979-987.
23. C. C. Bryden, C. N. Reilley and J. F. Desreux, *Anal. Chem.*, 2002, **53**, 1418-1425.
24. L. Wang, X. Zhu, X. Tang, C. Wu, Z. Zhou, C. Sun, S. L. Deng, H. Ai and J. Gao, *Chem. Commun.*, 2015, **51**, 4390-4393.
25. S. J. Moon, S. V. Govindan, T. M. Cardillo, C. A. D'Souza, H. J. Hansen and D. M. Goldenberg, *J. Med. Chem.*, 2008, **51**, 6916-6926.
26. Y. Pommier, *Nat. Rev. Cancer.*, 2006, **6**, 789-802.
27. Z. A. Rasheed and E. H. Rubin, *Oncogene*, 2003, **22**, 7296-7304.
28. J. H. Jang, W. R. Kim, A. Sharma, S. H. Cho, T. D. James, C. Kang and J. S. Kim, *Chem. Commun.*, 2017, **53**, 2154-2157.
29. L. Wang, H. Lin, L. Ma, J. Jin, T. Shen, R. Wei, X. Wang, H. Ai, Z. Chen and J. Gao, *Nanoscale*, 2017, **9**, 4516-4523.

View Article Online
DOI: 10.1039/C9CC01816F

# TOC

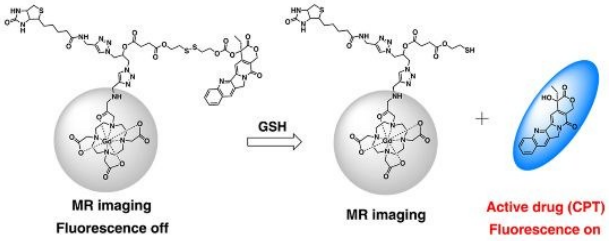


A molecular theranostic prodrug for treatment of tumour and real-time monitoring *via* MRI *in vivo* was reported.